

Probing dark energy inhomogeneities with supernovae

Michael Blomqvist¹, Edvard Mörtsell² and Serena Nobili²

¹ Department of Astronomy, Stockholm University, AlbaNova University Center
S-106 91 Stockholm, Sweden

² Department of Physics, Stockholm University, AlbaNova University Center
S-106 91 Stockholm, Sweden

E-mail: michaelb@astro.su.se, edvard@physto.se, serena@physto.se

Abstract. We discuss the possibility to identify anisotropic and/or inhomogeneous cosmological models using type Ia supernova data. A search for correlations in current type Ia peak magnitudes over a large range of angular scales yields a null result. However, the same analysis limited to supernovae at low redshift, shows a feeble anticorrelation at the 2σ -level at angular scales $\theta \approx 40^\circ$. Upcoming data from, e.g. the SNLS and the SDSS-II supernova searches will improve our limits on the size of – or possibly detect – possible correlations also at high redshift at the percent level in the near future. With data from the proposed SNAP satellite, we will be able to detect the induced correlations from gravitational lensing on type Ia peak magnitudes on scales less than a degree.

Keywords: dark energy theory, supernova type Ia

1. Introduction

Together with the identification of dark matter, the dominant question in cosmology today is what is responsible for the apparent acceleration of the universal expansion. Assuming that the cause is a dominant energy component with negative pressure, current efforts are focused on if this dark energy (DE) component can be described by a cosmological constant (CC), i.e. an energy component with constant density and a fixed equation of state (EOS) given by $p = \omega\rho$ where $\omega = -1$, or if dark energy is dynamical (DDE) with a varying EOS, $\omega = \omega(z)$.

Two main techniques are employed in these investigations; probing cosmological distances and probing the growth of cosmological structures, both of which are sensitive to the energy content of the universe. Distances are most robustly probed by type Ia supernovae (SNe Ia) [1, 2, 3, 4], the baryon acoustic oscillation (BAO) peak [5, 6, 7] and the last scattering surface of the cosmic microwave background (CMB) [8]. Structure growth is mainly probed by large galaxy surveys such as the 2dF [9] and the SDSS [10, 11] but also by galaxy cluster counts [12] and weak lensing [13]. Despite some claims of the contrary, there is a consensus that current data is perfectly consistent with

having approximately 70% of the energy density in the universe in the form of a CC [14].

However, cosmological distances only depend on the dark energy EOS in the form of a double integral and it is thus very difficult to investigate the time evolution of the EOS parameter, $w(z)$. Though not demanding it, current data thus still allows for large deviations of $w(z)$ from the CC value of $w = -1$ [14]. Even if the limits on $w(z)$ will improve in the future, detecting such an evolution remains notoriously difficult, especially if the deviation from the CC value turns out to be small.

It is thus of interest to look for alternative ways to detect or constrain any behaviour of the DE that differs from that of a CC. One such possibility is to study not temporal evolution, but rather spatial variations in DE properties. The CC value $w = -1$ is special in the sense that it not only gives a constant energy density in time, but also that it prevents any spatial clustering of DE. Any deviations from this value inevitably causes the DE to cluster, a clustering – which if detected – would refute the CC as the dominant energy component in the universe.

The clustering properties of DDE in different models and scenarios have been investigated in several recent articles (see, e.g., [15] and references therein). For values close to $w = -1$, such clustering is expected to be weak and take place mainly on very large scales, larger than the current Hubble radius and thus inaccessible for observations. On smaller scales, it can be shown that the DE density will tend to be anticorrelated with the matter density [15, 16]. Although, again, the amount of clustering is expected to be small (on the order of $10^{-5}[1 + w]$), it is nevertheless important to get observational confirmation that this indeed is the case, even if it is not expected from purely theoretical considerations. On a more speculative note, also in models where the apparent acceleration of the universe is explained in terms of the back-reaction of inhomogeneities in the universe, do we expect to have spatial variations in, e.g., cosmological distances [17]. Furthermore, cosmological observations can be used to put constraints on the degree of centricity in spherically symmetric inhomogeneous models [18, 19] and on anisotropic DE models [20, 21, 22, 23, 24].

One way to probe models with inhomogeneous DE or back-reaction, is to look for anisotropies in the observed peak magnitudes of SNe Ia. In general, we expect cosmological distances to be correlated on scales similar to the clustering scale of the DE or the matter inhomogeneities responsible for the back-reaction effect. The detection of such correlations is demanding because of the intrinsic variation and observational uncertainties in SN Ia peak magnitudes.

Since systematic effects connected to, e.g., the observational properties of different telescopes, calibration issues and details of the light-curve fitting procedure, can induce correlations on SN Ia magnitudes, it is important to minimize these effects by using as homogeneous data sets as possible in the analysis. Also, physical effects such as peculiar motions [25], gravitational lensing [26] and dust extinction [27] will introduce correlations in the SN Ia data and need to be controlled, and if possible, corrected for.

In Kolatt & Lahav (2001) [28], an early data set consisting of a total of 79

SNe Ia combined from the Supernova Cosmology Project [2] and the High- z Supernova Search Team [1] was used to look for directional variations in the best fit cosmological parameters. The result is consistent with the expected statistical variations in a homogeneous universe. Gupta et al. (2007) [29] used a more homogeneous set of 157 SNe Ia [30] to look for directional variations in the statistical scatter around the best fit cosmological model, again with a result consistent with null variations. A slightly different technique was used in Bochner (2007) [31] to look for anisotropic scatter in 172 SNe Ia [32] with similar results. Although current investigations have been mainly inconclusive, Schwartz & Weinhorst (2007) [33] find an off-set in the best fit calibration of low- z SNe Ia, between the North and South equatorial hemispheres at the 95% confidence level. Whether this hint of a North/South asymmetry is due to a statistical coincidence, observational systematic differences, correlated peculiar motions or has a cosmological origin is not clear at the moment.

In this paper we devise a general methodology of detecting angular correlations in SN Ia magnitude residuals. We apply this method to current SN Ia data as well as simulated upcoming data sets.

In Sec. 2, we describe the method for analysing SN Ia magnitude residuals for angular correlations and define the detection limit for such correlations. Two data sets from the literature are analysed for angular correlations in Sec. 3. In Sec. 4, we present different SN Ia surveys and investigate the detection limits for each of them. In Sec. 5, we assume a toy model correlation function and illustrate how future data can put limits on such a correlation. The paper is concluded in Sec. 6.

2. Method

In this paper we study angular correlations only, since the effect from possible DE inhomogeneities is larger in the transverse direction than in the radial direction. Moreover, a full three-dimensional study would require larger statistics than is currently available. The data sets we investigate contain both nearby and distant SNe Ia, for which we have redshifts, z , observed peak magnitudes, m_{obs} , with uncertainties, σ_m , as well as positions on the sky, right ascension, α , and declination, δ .

2.1. The angular correlation function

The magnitude residual of a SN Ia on the Hubble diagram is the difference between its observed magnitude and the magnitude predicted from its redshift in the best fit cosmology,

$$\delta m = m_{\text{obs}} - m_{\text{fit}} . \quad (1)$$

We define a normalized and scaled residual, X , by subtracting the mean and dividing by the uncertainty,

$$X \equiv \frac{\delta m - \mu_{\delta m}}{\sigma_m} . \quad (2)$$

Note that σ_m include both observational errors and the intrinsic dispersion of the SN Ia peak magnitudes. Thus, for uncorrelated Gaussian errors, we expect X to follow a normal distribution with mean, $\mu_X \approx 0$, and dispersion, $\sigma_X \approx 1$.

The angular correlation function of the magnitude residuals for a certain angular separation is defined as the expectation value of the product of the magnitude residuals of all SN pairs separated by that angle,

$$C(\theta) = \langle X \cdot X(\theta) \rangle , \quad (3)$$

where the angular separation, θ , between two SNe (denoted 1 and 2) is given by

$$\cos(\theta) = \sin(90^\circ - \delta_1) \sin(90^\circ - \delta_2) \cos(\alpha_1 - \alpha_2) + \cos(90^\circ - \delta_1) \cos(90^\circ - \delta_2) . \quad (4)$$

Note that our definition of the correlation function is equivalent to the correlation coefficient for the original residuals, δm ,

$$C(\theta) \equiv \rho_{\delta m \delta m(\theta)} . \quad (5)$$

If $C(\theta) > 0$, the magnitude residuals are correlated, if $C(\theta) = 0$ they are uncorrelated and if $C(\theta) < 0$ they are anticorrelated.

2.2. Detection limits for Gaussian magnitude residuals

Under the assumption that the magnitude residuals follow a Gaussian distribution with a mean of zero and a variance $\sigma_X^2 \approx 1$, their product will follow a probability density distribution given by

$$p(X \cdot X) = \frac{1}{\pi \sigma_X^2} K_0 \left(\frac{|X \cdot X|}{\sigma_X^2} \right) , \quad (6)$$

where K_0 is the modified Bessel function of the second kind and $X \cdot X$ denotes all possible products between the magnitude residuals. The variance of this probability density distribution is $\sigma_{X \cdot X}^2 = \sigma_X^4$.

The correlation for a given angular separation, is the expectation value of the product of the magnitude residuals for N_p number of SN pairs, where N_p is the number of unique pairs possible to define from a set of N SNe,

$$N_p = \frac{N^2 - N}{2} . \quad (7)$$

The dispersion in this expectation value is given by

$$\sigma_C = \frac{\sigma_{X \cdot X}}{\sqrt{N_p}} = \frac{\sigma_X^2}{\sqrt{N_p}} . \quad (8)$$

Since $\sigma_X^2 \approx 1$, we can define the n-standard deviation (n- σ) detection limit of the angular correlation to be

$$C_{\text{lim}} = \frac{n}{\sqrt{N_p}} . \quad (9)$$

3. Analysing current data for angular correlations

In this section, we will apply the methodology described above, on two current SN Ia data sets in order to search for possible angular correlations in the magnitude residuals. We again stress the importance of using as homogeneous data sets as possible in order to minimize the impact of systematic effects connected to, e.g., the light-curve fitting method used when deriving the peak magnitudes.

3.1. Data sets

The first year Supernova Legacy Survey (SNLS) data set in Astier et al. (2006) [3] (we will denote this data set astier06) contains a total of 115 SNe Ia, of which 71 are high- z SNLS SNe ($z > 0.2$) and 44 are nearby ones ($z < 0.2$). Figure 1 (left panel) shows the distribution of the SNe on the sky in galactic coordinates. Whereas the nearby SNe Ia (pluses) are scattered across the entire sky, the SNLS SNe (triangles) are confined to four pencil-beam patches, each covering a 1 square degree area. These patches are referred to as D1-D4 and contain 14, 8, 31 and 18 SNe, respectively. The SALT light-curve model was used to fit all the SN Ia light-curves in the data set. We add an intrinsic dispersion of $\sigma_{\text{int}} = 0.13$ to the uncertainties in the observed SN Ia magnitudes provided.

The second data set is from Davis et al. (2007) [14, 3, 4, 34] (we denote this davis07) and is a compilation of 192 SNe Ia consisting of 60 ESSENCE SNe, 57 SNLS SNe, 30 HST “gold” SNe and 45 nearby SNe. Figure 1 (right panel) shows the distribution of the SNe on the sky in galactic coordinates. Most of the low- z SNe (pluses) are the same as in astier06 and thus fairly equally distributed across the sky. The 147 high- z SNe (diamonds) are, on the other hand, very unevenly distributed. We use the peak magnitudes and uncertainties reported by davis07, which were obtained using the MCLS2k2 light-curve fitter on all photometric data. The uncertainties include both the observational and the intrinsic magnitude scatter.

Since the two data sets have many SNe in common, e.g., most of the nearby SNe, the corresponding correlation functions will not be independent. Comparison of the results will provide a useful check on the impact of the light-curve fitter used in deriving the SN Ia peak magnitudes on the angular correlation function.

3.2. Results

For a given data set, we find the best fit cosmological parameters, subtract the corresponding magnitudes, m_{fit} , from the observed magnitudes, m_{obs} , to get the residuals, δm . From these, we subtract the mean residual[‡], $\mu_{\delta m}$, and divide with the uncertainty, σ_m , to obtain the normalized and scaled magnitude residuals, X .

The values of the magnitude residuals and, consequently, the correlation function obviously depend to some degree on what cosmology we subtract. However, by varying

[‡] The value of $\mu_{\delta m}$ is very close to zero.

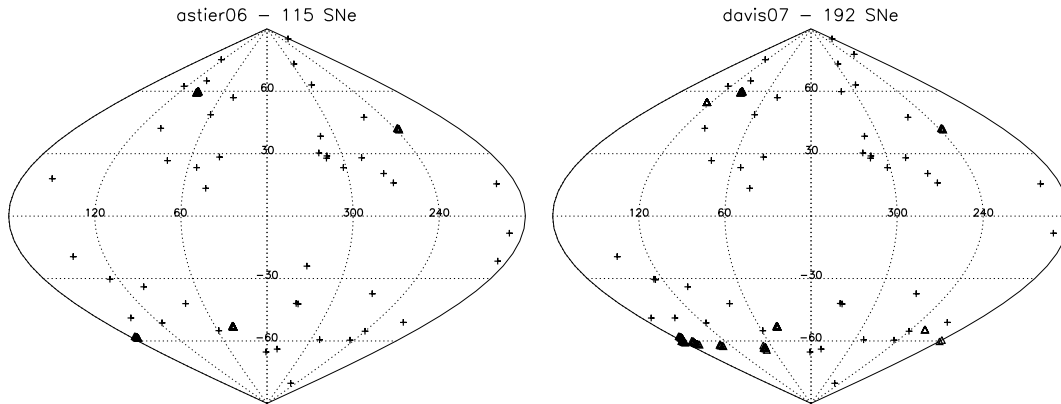


Figure 1. Distribution of SNe Ia on the sky in galactic coordinates. Left panel: 115 SNe Ia in astier06, consisting of 71 SNLS SNe (triangles) and 44 low- z SNe (pluses). Note the pencil beam geometry of the four SNLS survey patches. Right panel: 192 SNe Ia in davis07, with 147 high- z SNe (triangles) and 45 low- z SNe (pluses). Many of the SNe are the same as in astier06.

the cosmological parameters of the subtracted model, we have verified that the impact on the correlation function is very small.

The correlation functions for the 115 SNe Ia in astier06 and 192 SNe Ia in davis07 are presented in Figure 2. The error bars are obtained using Monte Carlo simulations where we generate 2000 new data sets by adding random numbers from a Gaussian distribution with a mean of zero and a variance of $\sigma_X^2 = 1$ to the magnitude residuals of the SNe Ia. These data sets are then analysed to investigate the possible spread in the correlation function. The error bars represent the 68% confidence limit. The data is binned in such a way that each bin contains approximately the same number of SN pairs with an angular resolution of approximately 15° . Note that since each SN Ia is included in several bins, the data points will not be independent from each other, as seen clearly in the right panel of Figure 2, where almost all the data are below the line. Thus, we do not expect about 1/3 of the points to lie more than 1σ away from the zero line, as would be the case for uncorrelated data points. The horizontal bars indicate the range of each bin and the points are placed at the average angular separation in each bin. Both data sets are clearly consistent with the SN magnitude residuals being uncorrelated, but allowing for correlations at the $\sim 10\%$ and $\sim 5\%$ level for the astier06 and davis07 sample respectively.

3.3. High- z

We expect the effects from inhomogeneous DE to be more prominent at large distances and also systematic effects from, e.g., peculiar velocities to decrease with distance. Therefore, we check the high- z SNe Ia in both astier06 and davis07 for correlations separately, i.e. we exclude the low- z SNe Ia in the analysis. The results are presented in Figure 3. The error bars represent the 68% confidence limit and are obtained using

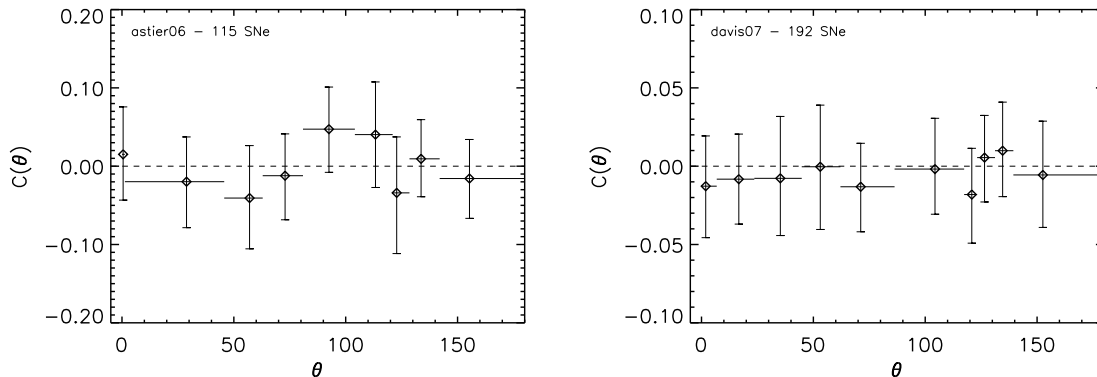


Figure 2. Correlation functions for the 115 SNe Ia in astier06 and the 192 SNe Ia in davis07. The error bars represent the 68% confidence limit. Each bin contains approximately the same number of SN pairs. The horizontal bars indicate the range of each bin and the points are placed at the average angular separation in each bin. Note that, the data points are not independent, since each SN contributes to several bins.

the same Monte Carlo simulations as above.

The left panel in Figure 3 shows the correlation function for the 71 SNLS SNe in astier06. Due to the pencil-beam geometry and the locations of the four patches of the SNLS survey, the SNe will be separated only by certain angles. We therefore do the binning at precisely these angles. The results are consistent with the SN magnitude residuals being uncorrelated. We note that there are differences in SN Ia brightness between the patches, e.g., there is a difference in the mean scaled magnitude residual between patch D1 and D4 of $X \approx 0.65$ (where D4 is the brighter), corresponding to a difference of $\langle \delta m \rangle \approx 0.11$ mag in the mean values of the original residuals. However, this is consistent with the expected statistical fluctuations at the 2σ -level. A search for correlations inside the patches, i.e. on sub-degree scales, yields a zero result for magnitude correlations also on small scales.

The right panel in Figure 3 shows the correlation function for the 147 high- z SNe in davis07 adopting a resolution of 22.5° . Again, the results are consistent with the SN magnitude residuals being uncorrelated.

3.4. Low- z

We also analyze the low- z SNe, in the redshift range $0.015 \leq z \leq 0.125$, separately. As noted, correlations between SNe Ia at low redshifts could be due to, e.g., correlations in their peculiar motions. However, since the SNe Ia in our sample are in the Hubble flow, we expect the contribution to the peak magnitude to be small. The results for the 44 nearby SNe in astier06 are presented in Figure 4 (left panel). The data is binned in such a way that each bin contains approximately the same number of SN pairs with an angular resolution of approximately 15° . We detect an anticorrelation at the 2σ -level

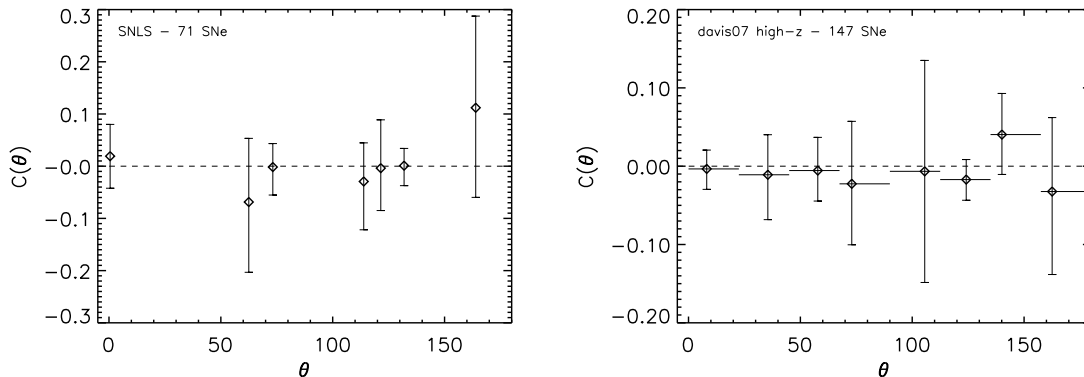


Figure 3. Correlation functions for the high- z SNe Ia in astier06 and davis07. The error bars represent the 68% confidence limit. Left panel: Correlation function for the 71 SNLS SNe in astier06. The bins are at the certain angular separations defined by the survey geometry. Right panel: Correlation function for the 147 high- z SNe in davis07. The binning is done uniformly. The horizontal bars indicate the range of each bin and the points are placed at the average angular separation in each bin.

around $\theta \approx 40^\circ$. The 45 low- z SNe in davis07 (out of which 41 SNe are also in astier06) show the same anticorrelation. Thus, we can exclude that this is an artefact of the fitting technique used for determining the peak magnitudes of the SNe. However, other systematic uncertainties, which are not included in the error bars, could contribute to decrease the significance of this detection.

In the right panel, we plot the scaled magnitude residuals, X , at every point on the sky by taking the weighted average of the residual for all SNe. The weight for each SNe is exponentially decreasing with respect to the distance to the point where the average is computed, using an exponential scale length of 15° .

4. Future data sets

As already noted, different SN surveys have very different survey geometries. The survey geometry affects the distribution of the angular separations which, in turn, affects on what scales and with what precision it is possible to detect possible correlations. We now consider the expected detection limit for SN Ia magnitude residual angular correlations for four different survey geometries, corresponding to the complete SDSS-II, SNLS and SNAP surveys as well as an all-sky survey.

4.1. SDSS-II

The SDSS-II§ (Sloan Digital Sky Survey) Supernova Survey’s survey area, called “Stripe 82” (southern equatorial stripe), is a 2.5 degree wide region along the celestial equator

§ www.sdss.org

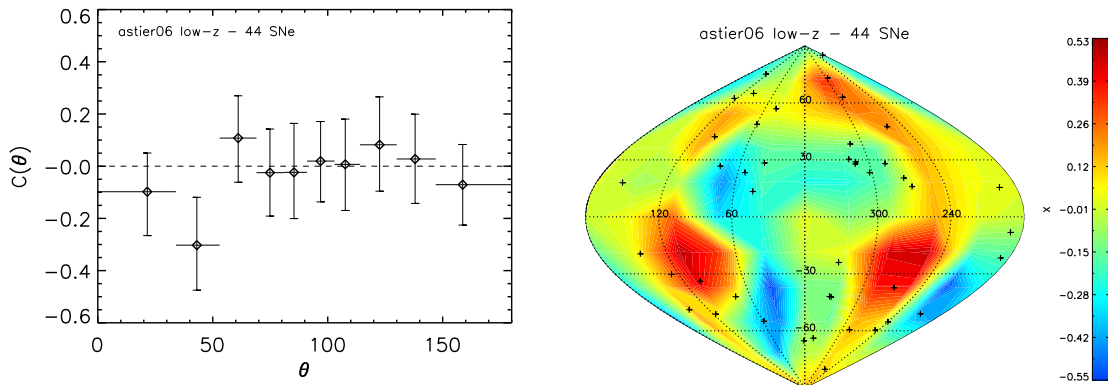


Figure 4. Left panel: Correlation function for the 44 low- z SNe in astier06. The error bars represent the 68% confidence limit. Each bin contains approximately the same number of SN pairs. The horizontal bars indicate the range of each bin and the points are placed at the average angular separation in each bin. Right panel: Colour map of the scaled magnitude residuals for the 44 low- z SNe in astier06 smoothed over an angular scale of 15° .

(i.e. $-1.25^\circ \leq \delta \leq 1.25^\circ$), from roughly $-60^\circ < \alpha < 60^\circ$. They aim of the survey is to find roughly 500 SNe Ia with $0.1 \lesssim z \lesssim 0.3$ in this area out of which 300 SNe Ia are expected to be used to build the Hubble diagram.

4.2. SNLS

The Supernova Legacy Survey^{||} (SNLS) is a pencil-beam survey, using four small square patches, each covering a 1 square degree area (see Figure 1 in Sec. 3.1 for the patch configuration). This is an example of a survey geometry that limits the detection of possible correlations to certain angular scales. One can either look for correlations inside the patches or between patches (six different combinations). Around 500 SNe Ia with redshifts up to $z \sim 1$ are expected to be used to build the final Hubble diagram.

4.3. SNAP

The survey geometry of the upcoming SNAP[¶] (SuperNova Acceleration Probe) satellite is not yet determined, but the plan is to cover a 7.5 square degree field in both the northern and southern hemisphere. In total, SNAP is expected to find 2000 SNe Ia with $z \lesssim 1.7$. We assume that the patches have a square geometry.

^{||} www.cfht.hawaii.edu/SNLS

[¶] snap.lbl.gov

4.4. All-sky

Pan-STARRS⁺ (Panoramic Survey Telescope & Rapid Response System) will as a by-product be able to detect a large number of SNe Ia across the entire sky. The proposed LSST* (Large Synoptic Survey Telescope) will search for faint astronomical objects across the entire sky and detect large amounts of SNe Ia. Depending on the observational effort put into following up these detections in the future, it is not unreasonable to assume that this could result in up to 2000 SNe Ia being put on the Hubble diagram at low- and mid- z within the next decade.

4.5. Results

We generate random SN positions in the ranges defined by the survey geometries and compute the $1\text{-}\sigma$ detection limits C_{lim} for each of the four surveys described above. In the results presented in Figure 5, we have assumed that the magnitude residuals in each bin correlate in the same way, i.e., the error bars do not reflect the fact that the correlation function may vary over the size of the bin.

The amplitudes and detailed shapes of the individual curves depend on the desired resolution. The lower the resolution, the larger the number of SN pairs in each bin and the lower the detection limit. We can scale the curves by making the crude estimate that the number of SN pairs in each bin scales with the bin size $\Delta\theta$ as $N_p \propto \Delta\theta$, such that C_{lim} decreases by a factor of \sqrt{K} if the resolution is degraded by a factor of K .

For the all-sky survey, there will be a peak at 90° in the distribution of the angular separations, with relatively few SN pairs at the smallest and largest separations. The all-sky survey thus probes correlations around $\theta = 90^\circ$ most effectively. In the top left panel of Figure 5, a resolution of 12° is assumed. The top curve is for a data set with 1000 SNe and the bottom curve for 2000 SNe.

For the SDSS-II, the angular separations are distributed with a maximum at small angles and then falls off for increasing separations. Beyond 120° it is not possible to probe possible correlations with this survey. In the top left panel of Figure 5, the two curves are for a data set with 300 SNe, with an angular resolution in the top curve of 10° and in the lower curve of 20° . The SDSS-II has its lowest detection limit at small angular scales.

Due to the pencil-beam geometry of the SNLS, it is only possible to probe certain discrete angular separations in this survey. We generate 125 SNe in each of the patches D1-D4 described in Sec. 3.1, for a total of 500 SNe. This means that there are equally many SN pairs in the bins, except for the first one, which probes correlations inside the patches. This bin contains more SN pairs and thus has the lowest detection limit as is evident from the lower left panel in Figure 5.

For the SNAP survey, we generate 1000 SNe in each patch, for a total of 2000 SNe. The distribution of the angular separations inside the patches resembles the shape for

⁺ pan-starrs.ifa.hawaii.edu

^{*} www.lsst.org

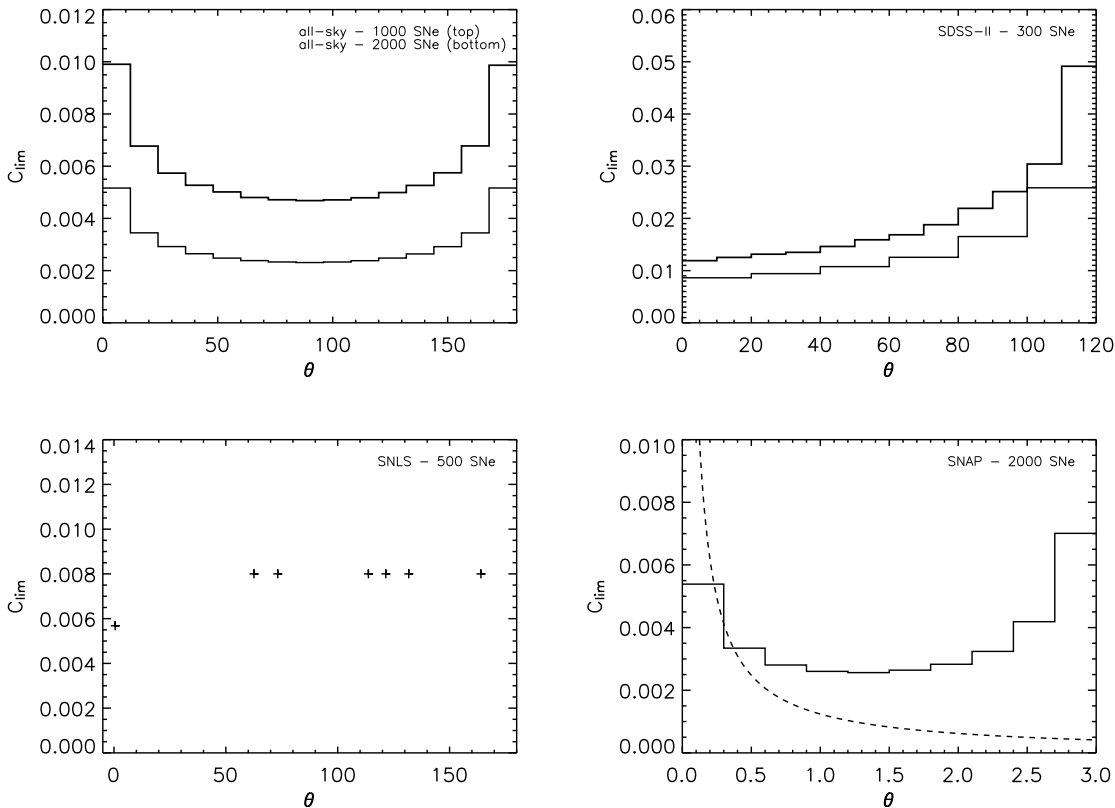


Figure 5. 1- σ detection limits for correlations in the magnitude residuals in different surveys. Top left panel: All-sky survey with 1000 SNe (top curve) and 2000 SNe (bottom curve). Top right panel: SDSS-II with 300 SNe for two different bin sizes. Bottom left panel: SNLS with 500 SNe. Note that the pencil-beam geometry only lets us probe certain discrete angular separations. Bottom right panel: SNAP with 2000 SNe for $\theta < 3^\circ$. The overplotted dashed line is the lensing correlation of Eq. (11) with $z_s = 1$.

the all-sky survey but with a small tail at the high end. In Figure 5 we have cut off the part of the distribution with $3^\circ < \theta < \sqrt{15}^\circ$ for readability reasons.

4.6. Lensing correlations

As noted in the introduction, physical effects such as peculiar motions and gravitational lensing will introduce correlations in the SN Ia data. Out of these, gravitational lensing will be the dominant contributor at $z \gtrsim 0.2$ [35]. The covariance of the weak lensing convergence κ for two sources at the same redshift z_s can be estimated by [36]

$$\langle \kappa \cdot \kappa(\theta) \rangle^{1/2} \approx 0.01 \sigma_8 \Omega_m^{0.75} z_s^{0.8} \left(\frac{\theta}{1^\circ} \right)^{-(n+2)/2}, \quad (10)$$

where n is the spectral index of the power spectrum of density fluctuations. For small convergence ($\kappa \ll 1$) the magnitude residual correlation due to weak lensing is given by

$$\langle X \cdot X(\theta) \rangle \approx \left(\frac{-5}{\ln(10)\sigma_m} \right)^2 \langle \kappa \cdot \kappa(\theta) \rangle \approx 10^{-3} \left(\frac{\sigma_m}{0.2} \right)^{-2} z_s^{1.6} \left(\frac{\theta}{1^\circ} \right)^{-1}, \quad (11)$$

where we have assumed $\sigma_8 = 0.8$, $\Omega_m = 0.3$ and $n = -1$. It is evident that correlations from gravitational lensing will only be important at small angular scales where we expect DE inhomogeneities to be negligible. A tentative detection of the effects of gravitational lensing on SNe Ia in the GOODS fields was made in Jönsson et al. (2007) [37] by cross correlating the SN Ia residuals with the lensing properties of foreground galaxies. The dense sampling of the SNAP survey fields will allow us to detect the angular correlation of SN Ia residuals without using the information from the lensing galaxies. In the bottom right panel of Figure 5, the lensing correlation for a source redshift of $z_s = 1$ (approximately equal to the average SN redshift expected for SNAP) and $\sigma_m = 0.2$ is compared with the SNAP correlation detection. It is clear that SNAP will be able to see the lensing correlation with a resolution of $< 0.3^\circ$; see also Ref. [38] for how this information can be used to probe cosmological parameters. We also note that with the increased statistics, it will be possible to probe the angular correlation function in separate redshift intervals, or to do a full three-dimensional correlation analysis.

5. Toy model

In this section, we assume a toy model angular correlation function, and illustrate how well we can detect such a correlation using future data expected for the SDSS-II and SNLS surveys described in Sec. 4. We let the magnitude residuals be the sum of an uncorrelated part, X_i , and a correlated part, X_c , due to, e.g., inhomogeneous DE,

$$X = X_i + X_c. \quad (12)$$

Our toy correlation function has the form of a Gaussian,

$$C(\theta) = A \exp\{-[(\theta - \theta_a)/\theta_c]^2\}, \quad (13)$$

where the amplitude, A , is the variance of the correlated magnitude residuals, $\sigma_{X_c}^2 = A$, θ_a is the angle where the correlation has its maximum value, and θ_c is the angular scale of the variation in the correlation function.

We generate random SN positions and uncorrelated intrinsic magnitude residuals with a mean of zero and a variance of $\sigma_{X_i}^2 = 1 - A$. The ratio of the dispersions of the intrinsic and the correlated magnitude residuals is

$$\frac{\sigma_{X_i}}{\sigma_{X_c}} = \sqrt{\frac{1 - A}{A}}. \quad (14)$$

Figure 6 shows the correlation function Eq. (13) with $\theta_c = 30^\circ$ and $\theta_a = 0^\circ$. The error bars represent the 68% confidence limit obtained from Eq. (9) for 300 SDSS-II SNe (triangles) and 500 SNLS SNe (diamonds). We have neglected the fact that the correlation function varies over the range of each bin. The binning is uniform for

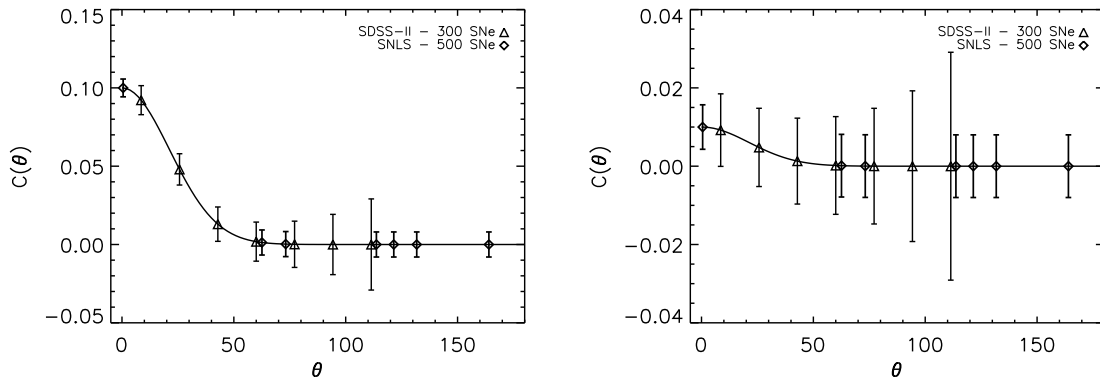


Figure 6. Our toy correlation function with $\theta_c = 30^\circ$ and $\theta_a = 0^\circ$ for 300 SDSS-II SNe (triangles) and 500 SNLS SNe (diamonds). The error bars represent the 68% confidence limit. Left panel: Correlation function amplitude $A = 0.1$, corresponding to $\sigma_{X_i}/\sigma_{X_c} = 3$. Right panel: $A = 0.01$, corresponding to $\sigma_{X_i}/\sigma_{X_c} \approx 10$. The SDSS-II has uniform binning while the SNLS correlation is evaluated at the seven discrete angular separations defined by the survey geometry.

the SDSS-II. For the SNLS, we have used the discrete angular separations defined by the survey geometry. The left panel shows the correlation function with $A = 0.1$, corresponding to $\sigma_{X_i}/\sigma_{X_c} = 3$. The correlation function is detected at high confidence using either data set. The right panel shows the correlation function with $A = 0.01$, corresponding to $\sigma_{X_i}/\sigma_{X_c} \approx 10$. The SDSS-II data set is not sufficient to detect the correlation in this case. For the SNLS, we expect to be able to make a weak detection of the correlation within the four survey patches.

6. Conclusions

The cosmological community is hard at work trying to constrain the behaviour of DE. The most pressing question is whether DE is a CC or something dynamical. A detection of temporal or spatial variations of DE would answer this question and refute the CC as the dominant energy component in the universe. At the same time, there are alternative attempts to explain the apparent acceleration of the universe without invoking DE at all, but instead originating in the large scale inhomogeneities in the matter distribution. Irrespective of their origin, large scale inhomogeneities would manifest themselves as anisotropies in the observed magnitudes of SNe Ia.

In this paper, we have devised a methodology of detecting angular correlations in SN Ia magnitude residuals. The methodology was applied to two recent data sets (astier06 and davis07), neither of which show any signs of correlations at angular scales $0^\circ < \theta < 180^\circ$. The uncertainties on the measured correlations, $C(\theta)$, are approximately 10% and 5% for the astier06 and davis07 data sets respectively, using an angular resolution of $\sim 15^\circ$. Note, however, that the two data sets are not independent, since

they overlap partially for the high redshift sample, and include almost the same set of nearby SNe. The main difference between the data sets is that different assumptions on SN Ia properties, such as intrinsic colour and dust extinction in the host galaxy, are used when deriving the SN Ia peak magnitudes. Such assumptions are responsible for some of the most important systematic uncertainties in SN Ia cosmology. A comparison between the results of the two data sets, allows us to keep the impact of these uncertainties on the measured correlation function under control. Because systematic uncertainties are typically different at low and high redshifts, and we expect effects from DE inhomogeneities to grow with redshift, we have applied the same analysis to both sub-samples separately. At low- z , we found an anticorrelation at the 2σ -level at angular scales $\theta \approx 40^\circ$. Due to the weak statistical significance of this detection, and the low redshifts, we cannot draw any conclusions about the possible implications for DE inhomogeneity. It is worth noticing that the nearby SNe analysed are a collection of very inhomogeneous data samples, collected by different observers at various telescopes and thus, there could be systematic uncertainties involved which have not been included in the error bars (see, e.g., discussion in [39]). We note that we see no signs of anisotropy on angular scales $\theta \sim 180^\circ$, corresponding to the North/South asymmetry detected in Ref. [33]. Our data sample, however, is only partially overlapping with that work, since we have only included SNe in the Hubble flow ($z \geq 0.015$) in our analysis in order to mitigate the effects from correlations arising from peculiar motions.

Gravitational lensing correlations will only be significant on small scales, where we expect the effects from DE clustering to be negligible. Using data from the proposed SNAP satellite, we should be able to detect the lensing correlations in SN Ia magnitudes with an angular resolution of $< 0.3^\circ$.

Correlations induced by intervening galactic dust will also mainly take place on very small angular scales, whereas correlations from dust in the Milky Way could potentially be a problem for an all-sky survey. Most surveys, however, observe in directions on the sky where the Milky Way dust extinction is well measured and understood.

More SN data is needed if we are to detect presumably weak correlations and better constrain inhomogeneous/anisotropic models. Our simulations of future data illustrate how the survey geometries govern on what scales, and to what precision, we will be able to detect possible angular correlations. We find that using data from the soon to be completed SDSS-II and SNLS surveys, we will typically be able to detect correlations in the magnitude residuals at the percent level.

Any claim of a deviation of DE properties from those of a CC will be subject to intense scrutiny from the cosmological community, and will need to be backed up by independent evidence in order to be generally accepted. It is therefore of utmost importance to pursue the study of DE along multiple paths. Although observationally demanding, the search for spatial variations in DE properties is a useful complement to studies aiming at constraining the time evolution of DE. Specifically, for SNe Ia, we expect systematic effects connected to the time evolution of DE, such as temporal evolution of SN Ia properties, to be of less importance when studying spatial variations

of DE. Since systematic effects constitute the limiting factor for future SN Ia surveys, we expect interesting results for the spatial correlations of SN magnitudes in the near future, irrespective of whether such correlations are found or not.

Acknowledgments

MB acknowledges support from the HEAC Centre funded by the Swedish Research Council. EM acknowledges support for this study by the Swedish Research Council and from the Anna-Greta and Holger Crafoord fund. The authors would like to thank Ariel Goobar for useful discussions.

References

- [1] Riess A G *et al* , *Observational Evidence from Supernovae for an Accelerating Universe and a Cosmological Constant*, 1998 *Astron. J.* **116** 1009
- [2] Perlmutter S *et al* , *Measurements of Omega and Lambda from 42 High-Redshift Supernovae*, 1999 *Astrophys. J.* **517** 565
- [3] Astier P *et al* , *The Supernova Legacy Survey: measurement of Ω_M , Ω_Λ and w from the first year data set*, 2006 *Astron. Astrophys.* **447** 31
- [4] Wood-Vasey W M *et al* , *Observational Constraints on the Nature of Dark Energy: First Cosmological Results from the ESSENCE Supernova Survey*, 2007 *Astrophys. J.* **666** 694
- [5] Cole S *et al* , *The 2dF Galaxy Redshift Survey: power-spectrum analysis of the final data set and cosmological implications*, 2005 *Mon. Not. R. Astron. Soc.* **362** 505
- [6] Eisenstein D J *et al* , *Detection of the Baryon Acoustic Peak in the Large-Scale Correlation Function of SDSS Luminous Red Galaxies*, 2005 *Astrophys. J.* **633** 560
- [7] Percival W J *et al* , *Measuring the Baryon Acoustic Oscillation scale using the Sloan Digital Sky Survey and 2dF Galaxy Redshift Survey*, 2007 *Mon. Not. R. Astron. Soc.* **381** 1053
- [8] Komatsu E *et al* , *Five-Year Wilkinson Microwave Anisotropy Probe (WMAP) Observations: Cosmological Interpretation*, 2008 Preprint 0803.0547 [astro-ph]
- [9] Hawkins E *et al* , *The 2dF Galaxy Redshift Survey: correlation functions, peculiar velocities and the matter density of the Universe*, 2003 *Mon. Not. R. Astron. Soc.* **346** 78
- [10] Pope A C *et al* , *Cosmological Parameters from Eigenmode Analysis of Sloan Digital Sky Survey Galaxy Redshifts*, 2004 *Astrophys. J.* **607** 655
- [11] Percival W J *et al* , *The Shape of the Sloan Digital Sky Survey Data Release 5 Galaxy Power Spectrum*, 2007 *Astrophys. J.* **657** 645
- [12] Dahle H, *The Cluster Mass Function from Weak Gravitational Lensing*, 2006 *Astrophys. J.* **653** 954
- [13] Hoekstra H *et al* , *First Cosmic Shear Results from the Canada-France-Hawaii Telescope Wide Synoptic Legacy Survey*, 2006 *Astrophys. J.* **647** 116
- [14] Davis T M *et al* , *Scrutinizing Exotic Cosmological Models Using ESSENCE Supernova Data Combined with Other Cosmological Probes*, 2007 *Astrophys. J.* **666** 716
- [15] Mota D F, Shaw D J and Silk J, *On the Magnitude of Dark Energy Voids and Overdensities*, 2007 *Astrophys. J.* **675** 29
- [16] Dutta S and Maor I, *Voids of dark energy*, 2007 *Phys. Rev. D* **75** 063507
- [17] Marra V, Kolb E W and Matarrese S, *Light-cone averages in a Swiss-cheese universe*, 2008 *Phys. Rev. D* **77** 023003
- [18] Enqvist K and Mattsson T, *The effect of inhomogeneous expansion on the supernova observations*, 2007 *J. Cosmol. Astropart. Phys.* JCAP02(2007)019

- [19] Alnes H and Amarzguioui M, *Supernova Hubble diagram for off-center observers in a spherically symmetric inhomogeneous universe*, 2007 *Phys. Rev. D* **75** 023506
- [20] Koivisto T and Mota D F, *Accelerating Cosmologies with an Anisotropic Equation of State*, 2007 *Astrophys. J.* **679** 1
- [21] Manera M and Mota D F, *Cluster number counts dependence on dark energy inhomogeneities and coupling to dark matter*, 2006 *Mon. Not. R. Astron. Soc.* **371** 1373
- [22] Rodrigues D C, *Anisotropic cosmological constant and the CMB quadrupole anomaly*, 2008 *Phys. Rev. D* **77** 023534
- [23] Mota D F *et al* , *Constraining dark energy anisotropic stress*, 2007 *Mon. Not. R. Astron. Soc.* **382** 793
- [24] Takada M, *Can a galaxy redshift survey measure dark energy clustering?*, 2006 *Phys. Rev. D* **74** 043505
- [25] Haugbølle T *et al* , *The Velocity Field of the Local Universe from Measurements of Type Ia Supernovae*, 2007 *Astrophys. J.* **661** 650
- [26] Cooray A, Huterer D and Holz D E, *Problems with Small Area Surveys: Lensing Covariance of Supernova Distance Measurements*, 2006 *Phys. Rev. Lett.* **96** 021301
- [27] Zhang P and Corasaniti P S, *Cosmic Dust Induced Flux Fluctuations: Bad and Good Aspects*, 2007 *Astrophys. J.* **657** 71
- [28] Kolatt T S and Lahav O, *Constraints on cosmological anisotropy out to $z = 1$ from Type Ia supernovae*, 2001 *Mon. Not. R. Astron. Soc.* **323** 859
- [29] Gupta S, Deep Saini T and Laskar T, *Direction Dependent Non-gaussianity in High- z Supernova Data*, 2007 Preprint [astro-ph/0701683]
- [30] Riess A G *et al* , *Type Ia Supernova Discoveries at $z > 1$ from the Hubble Space Telescope: Evidence for Past Deceleration and Constraints on Dark Energy Evolution*, 2004 *Astrophys. J.* **607** 665
- [31] Bochner B, *Looking for signs of Anisotropic Cosmological Expansion in the High- z Supernova data*, 2007 Preprint [astro-ph/0702730]
- [32] Tonry J L *et al* , *Cosmological Results from High- z Supernovae*, 2003 *Astrophys. J.* **594** 1
- [33] Schwarz D J and Weinhorst B, *(An)isotropy of the Hubble diagram: comparing hemispheres*, 2007 *Astron. Astrophys.* **474** 717
- [34] Riess A G *et al* , *New Hubble Space Telescope Discoveries of Type Ia Supernovae at $z > 1$: Narrowing Constraints on the Early Behavior of Dark Energy*, 2007 *Astrophys. J.* **659** 98
- [35] Bonvin C, Durrer R and Gasparini M A, *Fluctuations of the luminosity distance*, 2006 *Phys. Rev. D* **73** 023523
- [36] Mellier Y, *Dark Matter from Weak Gravitational Lensing*, 2002 *Space Science Reviews* **100** 73
- [37] Jönsson J *et al* , *Tentative detection of the gravitational magnification of Type Ia supernovae*, 2007 *J. Cosmol. Astropart. Phys.* JCAP06(2007)002
- [38] Cooray A, Holz D E and Huterer D, *Cosmology from Supernova Magnification Maps*, 2006 *Astrophys. J. L.* **637** L77
- [39] Nobili S *et al* , *The intrinsic colour dispersion in Type Ia supernovae*, 2003 *Astron. Astrophys.* **404** 901